LAWRENCE
LIVERMORE
NATIONAL
LABORATORY

UCRL-JRNL-222408

Correlation Spectroscopy of Minor Species: Signal Purification and Distribution Analysis

T. A. Laurence, Y. Kwon, E. Yin, C. Hollars, J. A. Camarero, D. Barsky

June 26, 2006

Biophysical Journal

This un-edited manuscript has been accepted for publication in Biophysical Journal and is freely available on BioFast at http://www.biophysj.org. The final copyedited version of the paper may be found at http://www.biophysj.org.

Correlation Spectroscopy of Minor Fluorescent Species: Signal Purification and Distribution Analysis

Ted A. Laurence*, Youngeun Kwon, Eric Yin, Christopher W. Hollars, Julio A. Camarero, and Daniel Barsky

Chemistry, Materials, and Life Sciences, Lawrence Livermore National Laboratory, Livermore, CA, USA

*to whom correspondence should be addressed (laurence2@llnl.gov)

Abstract

We are performing experiments that use fluorescence resonance energy transfer (FRET) and fluorescence correlation spectroscopy (FCS) to monitor the movement of an individual donor-labeled sliding clamp protein molecule along acceptor-labeled DNA. In addition to the FRET signal sought from the sliding clamp-DNA complexes, the detection channel for FRET contains undesirable signal from free sliding clamp and free DNA. When multiple fluorescent species contribute to a correlation signal, it is difficult or impossible to distinguish between contributions from individual species. As a remedy, we introduce "purified FCS" (PFCS), which uses single molecule burst analysis to select a species of interest and extract the correlation signal for further analysis. We show that by expanding the correlation region around a burst, the correlated signal is retained and the functional forms of FCS fitting equations remain valid. We demonstrate the use of PFCS in experiments with DNA sliding clamps. We also introduce "single molecule FCS", which obtains diffusion time estimates for each burst using expanded correlation regions. By monitoring the detachment of weakly-bound 30-mer DNA oligomers from a single-stranded DNA plasmid, we show that single molecule FCS can distinguish between bursts from species that differ by a factor of 5 in diffusion constant.

Keywords: Single molecule fluorescence spectroscopy, fluorescence correlation spectroscopy, fluorescence fluctuation spectroscopy

Introduction

Fluorescence correlation spectroscopy (FCS) (1) probes dynamical processes in fluorescent species over the large range of time scales from nanoseconds to seconds. By introducing a sufficiently small confocal volume to FCS, single molecules can be detected (2), and the applications of FCS to analysis of biological processes have thereby multiplied (3). FCS has been proposed as a way to analyze rare species (4, 5). Unfortunately, its usefulness can be limited in cases where multiple fluorescent species contribute to the same detection channel, contaminating the signal from a species of interest. If the dynamical processes of the contaminating species occur on similar time scales with the species of interest, it is very difficult and sometimes impossible to distinguish between contributions from different species. The correlation function for any minor species is obscured by contributions from other, more abundant species.

For example, we are performing solution-based single molecule experiments that monitor a DNA sliding clamp protein as it moves on DNA (β clamp of *E. coli*), by monitoring fluorescence energy transfer (FRET) between a donor (D) fluorophore on the β clamp and an acceptor (A) at a specific location on a DNA plasmid. FRET is caused by the non-radiative transfer of excitations from D to A when they are in close proximity (within ~5 nm). We perform these single-molecule FRET measurements of the dynamic complex of the β clamp on DNA using alternating laser excitation (ALEX) (6) in the presence of free plasmids and free β clamp proteins. With ALEX, three photon streams or channels are available: photons detected from donor fluorescence resulting from excitation by the donor excitation laser (hereafter, "donor channel"); acceptor-emitted photons detected in the acceptor channel that are the result of FRET excited by the donor excitation laser ("FRET channel"); and photons detected in the acceptor channel, that are the result of acceptor fluorescence, excited by the acceptor excitation laser ("acceptor channel"). In addition to signals from complexes undergoing FRET, the FRET channel contains contaminating signals caused by leakage of the donor emission into the acceptor channel and by direct excitation of the acceptor by the donor excitation laser (Figure 1). Although both of these problems must be considered, the former is amplified in our experiments by aggregates of the β clamp protein causing bright fluorescence bursts that leak into the acceptor channel. These bright bursts can appear indistinguishable from bursts caused by actual FRET. Autocorrelations performed on the FRET channel, therefore, have contributions from FRET and these contaminating sources, calling into question any conclusions drawn from correlation analysis, especially in the case where complexes are observed less frequently than the free components.

The cross-correlation (7) between the FRET channel and the acceptor channel obtained from the acceptor laser excitation (8) eliminates contributions from the free protein and aggregates since those species are not excited by the acceptor excitation laser. However, fluctuations in FRET efficiency, which should reveal the protein-DNA intermolecular movement sought in these experiments, are unobservable by a cross-correlation between the FRET channel and acceptor channel. This is because the acceptor signal excited by the acceptor laser is only correlated with diffusion in and out of the detection volume, not fluctuations in the FRET efficiency. Hence, this cross-correlation reflects only the fluctuations caused by the translational diffusion of the complexes in and out of the detection volume.

Solution-based single-molecule fluorescence spectroscopy (SMFS) uses ratiometric variables and fluorescence lifetime measurements to allow for the identification and sorting of many species in complex mixtures (9-12). Signals from single molecules are detected by searching for "bursts" of photons with signal intensities above a preset threshold level, determined by the background levels and expected signal intensities. The recently introduced alternating laser excitation (ALEX) of single molecules allows sorting of species based on distance and association (6, 13). Using ALEX, β clamp-DNA complexes are easily distinguished from free components by searching for fluorescence bursts in the FRET channel. Only those bursts that have coincident bursts in the FRET channel and in the acceptor channel are due to complexes. Any burst with a coincident large burst in the donor channel is due to a β clamp aggregate.

Although SMFS and FCS often use the same experimental setups and samples, techniques that take advantage of the power of SMFS to sort species while simultaneously using the ability of FCS to probe temporal dynamics remain underdeveloped. Selective fluorescence spectroscopy (SFS) (10), which selects single molecule bursts for further correlation analysis, is the most advanced technique in this direction. The region over which the correlation is calculated is truncated at the beginning and end of the burst, allowing for analysis of fluctuations within the timescale of the bursts. In order to maximize the time scales monitored using the correlation analysis, only the brightest (> 200 kHz) and longest single molecule bursts (>70 ms) are selected. These exceptional bursts correspond to fluorescent molecules that remain in the detection volume the longest. Nevertheless, the truncation used in the analysis prevents correlation analysis of fluctuations on the same time scale of the burst, including, for example, translational diffusion into and out of the optical detection volume.

The approach taken here also uses a selection of bursts, but it differs from SFS in two ways. First, the burst selection criteria are not as restrictive; we use much lower thresholds (5 – 15 kHz thresholds are typical), and allow much shorter bursts, only requiring sufficient signal over a 10 ms time bin. More importantly, the correlation calculations are not truncated at the burst edges. By expanding the region of the correlation around detected bursts, we introduce a way to use SMFS sorting to analyze temporal dynamics of specific species, including translational diffusion into and out of the optical detection volume, using standard FCS fitting equations (14, 15). Truncation of the signal is moved to regions uncorrelated with the signal from the selected burst, allowing the functional forms of FCS fitting functions to remain unchanged except for a multiplicative factor.

Thus, by selecting only those bursts that are due to the species of interest and averaging the resulting correlations over all selected bursts, we can "purify" the signal of interest. This purification eliminates contributions both from leakage of the donor emission into the acceptor channel and direct excitation of the acceptor (Figure 1). Due to the exclusion of contaminating signals, autocorrelations of the FRET channel calculated after signal purification may be used to study the fluctuations of an individual species. Signal purification may also be used for photon arrival-time interval distribution (PAID) functions (16) in the same way as for FCS. We call our method of purifying correlations signals by performing correlations over selected bursts "purified FCS," or PFCS. We

will refer to performing correlations only over the photons in the truncated single molecule bursts without correlation region expansion as selective FCS, or SFCS.

Here we demonstrate the use of PFCS using our β clamp-DNA experiments. We also investigate how precisely a diffusion time can be extracted from the correlation calculated for a single burst. We call the method of analyzing FCS for single molecule bursts "single molecule FCS." Here, single molecule FCS will be applied to experiments containing two species—one of free labeled DNA oligomers, the other of those oligomers hybridized to ssDNA plasmids. In this application of our method we show that many DNA oligomers weakly bound to plasmids during hybridization reactions with excess DNA oligomer are removed by gentle heating (at 37 ºC) of diluted solutions of the hybridized DNA.

Theory

Purified FCS with correlation region expansion

We illustrate our new method through a simulation of an experiment of two interacting proteins, as shown in Figure 2. In the simulated experiment, we monitor the fluctuations of the emission in the FRET channel from the intermolecular interaction between a protein labeled with a donor fluorophore D and a second protein labeled with an acceptor fluorophore A (Species 1 in Figure 2). The emission in the FRET channel is contaminated by the presence of aggregates of the D-labeled species (Species 2 in Figure 2). The D emission from Species 2 leaks into the FRET detection channel, leading to bursts that appear similar to those from Species 1 (the acceptor detection channel excited by the acceptor excitation laser is not simulated). Using values chosen to correspond roughly to the values found in our β clamp experiments, Species 1 and 2 are both present with a molecular occupancy of $c_1 = c_2 = 0.05$ in the detection volume, and a molecular brightness of $q_{1,\mathrm{FRET}} = q_{2,\mathrm{FRET}} = 35$ kHz in the FRET channel. The molecular brightness is the number of photon counts per second received from a single fluorescent molecular, averaged over the confocal detection volume. In the donor channel, Species 2 has a brightness of $q_{2,\mathrm{D}} = 141$ kHz and Species 1 has a brightness of $q_{1,\mathrm{D}} = 0$ kHz (the leakage of A into the donor channel is negligible, and will not be considered further). Due to translational diffusion through the optical detection volume, each molecular species is associated with a characteristic "diffusion time," i.e., the average time a molecule remains in the detection volume. The diffusion times are $\tau_{D,1} = 3$ ms and $\tau_{D,2} = 6$ ms for Species 1 and 2, respectively. Species 2 is distinguished from Species 1 by the presence or absence of a coincident burst in the donor channel.

Bursts from Species 1 and 2 are distinguished using single molecule fluorescence analysis. Single-molecule fluorescence bursts are identified using the burst search method described in (6), with the addition of a median-based background subtraction (Materials and Methods). A histogram of FRET efficiency ratio *E* (proximity ratio) for all bursts (17) clearly shows two subpopulations (figure 2b).

Additional information may be gleaned from these bursts by calculating correlations on the photons contained in the bursts. The temporal cross-correlation function is defined as

$$C_{AB}(\tau) \equiv \langle I_A(t) I_B(t+\tau) \rangle / \langle I_A(t) \rangle \langle I_B(t+\tau) \rangle \quad (1)$$

, where $I_A(t)$ and $I_B(t)$ are detected intensities for channels *A* and *B*, and t and τ are continuous time and time lag variables. For a single fluorescent species diffusing within a Gaussian detection volume, the correlation function for FCS follows the equation (18),

$$C_{AB}(\tau) = 1 + \frac{1}{c} \frac{1}{1+\tau/\tau_D} \sqrt{\frac{1}{1+\tau/(K\tau_D)}} \quad (2)$$

c is the average number of fluorescent species in the confocal detection volume, τ_D is the diffusion time of the species, and *K* is the square of the ratio between the ratio between the width of Gaussian detection volume along the optical axis and the width of the volume perpendicular to the optical axis (25 for our simulations). In experiments with relatively large pinholes, actual detection volumes are not Gaussian, and Equation (2) generally works equally well without the square root term (14). Additional terms can be added to Equation (2) for additional species, but they must now account for differences in brightness for each species,

$$C_{AB}(\tau) = 1 + \left[\sum_{i=1}^{M} c_i q_{A,i} q_{B,i} \frac{1}{1+\tau/\tau_{D,i}} \sqrt{\frac{1}{1+\tau/(K\tau_{D,i})}} \right] \Bigg/ \left[\left(k_A + \sum_{i=1}^{M} c_i q_{A,i} \right) \left(k_B + \sum_{i=1}^{M} c_i q_{B,i} \right) \right] \quad (3)$$

M is the number of species. For each species *i*, there is the molecular occupancy c_i, the brightness in channels A and B, $q_{A,i}$ and $q_{B,i}$, and diffusion time $\tau_{D,i}$. There are also background count rates in both channels, k_A and k_B. The relative contributions to the correlation function can be quantified by comparing the correlation amplitudes $c_i q_{A,i} q_{B,i}$ from each species.

The data recorded for photon-timing SMFS/FCS experiments are series of photon time stamps with time resolution Δt. t_i is the arrival time of the i^{th} photon from channel *A*, and u_j is the arrival time of the j^{th} photon from channel *B*. Assuming stationarity, the ensemble averages in the expression for $C_{AB}(\tau)$ are converted to averages over all time. Averaging over a finite experimental time T with N_A and N_B photons detected in the respective channels gives a correlogram $\hat{C}_{AB}(\tau)$, an estimate of the actual correlation function.

In terms of discrete photon time stamps t, $I_A(\mathrm{t})$ is the number of photons i such that $\mathrm{t}=\mathrm{t}_i$; or $I_A(\mathrm{t}) = n\left(\{i | \mathrm{t}_i = \mathrm{t}\}\right)/\Delta t$, where $\{i | \mathrm{t}_i = \mathrm{t}\}$ is the set of all photons i such that $\mathrm{t}_i=\mathrm{t}$, and the operator n counts the number of elements in the set. Similarly, we have $I_B(\mathrm{t}) = n\left(\{j | \mathrm{u}_j = \mathrm{t}\}\right)/\Delta t$. In this notation, using discrete time lag τ, Equation (1) becomes

$$\hat{C}_{AB}(\tau) = \frac{n\left(\left\{(i,j)\middle|\mathrm{t}_i = \mathrm{u}_j - \tau\right\}\right)(T-\tau)}{n\left(\left\{i\middle|\mathrm{t}_i \le T-\tau\right\}\right)n\left(\left\{j\middle|\mathrm{u}_j \ge \tau\right\}\right)}. \quad (4)$$

$\left\{(i,j)\middle|\mathrm{t}_i = \mathrm{u}_j - \tau\right\}$ is the set of all photon pairs, (i,j) such that $\mathrm{t}_i = \mathrm{u}_j - \tau$. The restrictions on the average intensities in the denominator are for symmetric normalization (19).

We use single-molecule ratiometric measurements to select a species of interest. If there are *N* bursts selected, then we average the correlations for all *N* bursts to obtain the accurate correlation for the species. For the k^{th} burst, we have the photons t_{ki} and u_{kj} in channels *A* and *B*, which occur over a burst duration T_k. The correlation functions are combined according to the following:

$$\hat{C}_{AB}(\tau) = \frac{\sum_k n\left(\left\{(i,j)\middle|\mathrm{t}_{ki} = \mathrm{u}_{kj} - \tau\right\}\right)\sum_k (T_k - \tau)}{\sum_k n\left(\left\{i\middle|\mathrm{t}_{ki} \le T_k - \tau\right\}\right)\sum_k n\left(\left\{j\middle|\mathrm{u}_{kj} \ge \tau\right\}\right)} \quad (5)$$

If we combine correlations performed only on photons within bursts, the functional forms for the correlation do not match the FCS fitting equation in Equation (2) on time scales near the burst width (Figure 2c). The autocorrelation of the FRET channel for the whole experiment fits well to the single-component FCS model in Equation (2) with a diffusion time of 4.2±0.1 ms (black squares, simulation data; black line, fit). FCS was not able to distinguish the two diffusing species present with a factor of 2 difference in diffusion times. Using selective FCS (truncating correlations at burst edges) for all of the bursts from Species 1 or Species 2, we find a difference in the diffusion time between the two species (light gray circles and dark gray triangles in Figure 2c). The autocorrelation of the FRET channel for bursts from Species 1 (dark gray region in Figure 2b) is fit by Equation (2) with a diffusion time of 1.7±0.1 ms (dark gray triangles and curve in Figure 2c). The autocorrelation of the FRET channel for bursts from Species 2 (light gray region in Figure 2b) is fit by Equation (2) with a diffusion time of 3.3±0.1 ms (light gray circles and curve in Figure 2c). Unfortunately, both fits are poor, and the extracted values do not match the simulation values put in.

The primary problem encountered in Figure 2c is that burst searching routines select only those parts of the signal that are bright. The selected time regions have widths on the same time scale as the diffusion time, truncating a significant amount of correlated signal. In order to properly characterize the signal fluctuations, the time scale over which the correlation function is performed must be longer than the time scale of the fluctuations themselves. We introduce a simple way to do this: expand the region of the correlation function around the burst so that the region has a time width much longer than the diffusion time (see figure 2d). We expand it here by 10-fold (i.e. 100 ms) on either side of each burst. We expand enough to allow the correlation functions calculated to have the same functional form as standard FCS fitting model in Equation (2). We do not expand too much, so that we can exclude unwanted single molecule bursts from other species. We also want to exclude contributions from more persistent fluctuating signals,

such as leakage from low intensity, higher concentration signals. The correlations are calculated as in Eq. (5), except that now k is an index for expanded correlation regions rather than just the time of the bursts.

There is one change in the functional form in Equation (2) for purified FCS due to the selection only of regions with bursts. FCS detects the molecular occupancy by comparing the variance and mean of the signal intensity. We are selecting regions that contain single molecule bursts, so the mean and variance of the signal intensity of the selected regions are different from the mean and variance for the entire experiment. Hence, the normalization as shown in Eq. (5) does not work properly. We use a multiplicative correction factor a as a parameter in all of our fits, accounting for this problem.

There are two uses for the expanded correlation regions for selected bursts. First, one may select only those correlation regions containing bursts of a specific species, excluding bursts from other species as well as leakage of higher concentration species into the channel of interest. The correlations for all regions can be averaged according to Eq. (5), obtaining the purified correlation function for a selected species. This methodology is an example of the use of single-molecule fluorescence to sort molecules for later sub-ensemble analysis (13). Second, one may fit the correlations for individual regions to an FCS model, and the distribution of fitted diffusion times may be used to directly observe the distribution of diffusion times in the sample. This "single molecule FCS" is described later.

There are two clear limitations to this method. First, PFCS is limited to cases where the methods of single molecule spectroscopy can distinguish the species involved; there must be some distinguishing parameter such as E that clearly reveals two or more subpopulations. Second, the concentration of fluorescent molecules monitored must be low so that bursts from multiple species are not included in the correlation region. In the correlation function example, handling cases where only one or two additional bursts are within the expanded correlation region is not difficult. In Figure 2d, the correlation region was expanded around the central burst from Species 1, and includes an additional, earlier burst. Since that burst is also from Species 1, that region is included in the analysis. However, in Figure 2e the expanded correlation region included a burst from Species 2, and that region is excluded from the analysis. Similar rules can be developed for a specific experimental situation.

Figure 2f shows that the purified correlations calculated for Species 1 and 2 match the correlations expected for those species if they were alone in solution. The correlation function for regions of interest containing bursts from Species 1 (dark gray region in Figure 2b) is well fit by a single-component model with a diffusion time of 3.0±0.1 ms (dark gray triangles and curve in Figure 2f). The correlation function for regions of interest containing bursts from Species 2 (light gray region in Figure 2b) is well fit by a single-component model with a diffusion time of 5.6±0.1 ms (light gray circles and curve in Figure 2f). The fitted values for the diffusion times are within 10% of the simulation input values.

Another situation in which PFCS may be used is where Species 1 is again a complex undergoing FRET at single molecule concentrations, but Species 2' is a non-aggregated

donor-labeled protein present at higher concentrations. The donor emission from Species 2' again leaks into the FRET channel, but now presents a low-intensity, fluctuating background that contributes to the FRET autocorrelation function. For PFCS to work in this situation, the species of interest must be significantly brighter than the fluctuating background. For these simulations, we used the same parameters for Species 1 as before, but with a lower molecular occupancy of $c_1 = 0.02$. We replace Species 2 with Species 2', the molecular occupancy is $c_{2'} = 2.5$, the brightness in the FRET Channel is $q_{1,\mathrm{FRET}} = 2.3$ kHz (15 times smaller than for Species 1), and the diffusion time is $\tau_{D,2'} = 600\ \mu$s. By selecting correlation regions around large fluorescence bursts in the FRET channel (as shown in Figure 2), we effectively concentrate the signal of interest, excluding most of the experimental time where only the leakage signal from Species 2' is present. The relative contribution of each species to the amplitude of the autocorrelation function of the FRET channel can be calculated as $A_i = c_i q_{i,\mathrm{FRET}}^2$, the contribution to the numerator in Equation (3). For the autocorrelation of the FRET channel for the whole experiment, the amplitudes are $A_1 = 24.5$ kHz^2 and $A_2 = 13.6$ kHz^2. After using PFCS, the amplitudes are $A_1 = 183$ kHz^2 and $A_2 = 13.6$ kHz^2, increasing the contribution of Species 1 to the correlation amplitude from 64% to 93% of the total correlation amplitude. For the autocorrelation of the FRET channel over the whole simulated experiment, we obtain a diffusion time of 2.1 ± 0.1 ms with a poor fit to Equation (2). Using PFCS to exclude most of the fluctuating background, we obtain a good fit to the autocorrelation of the FRET channel with a diffusion time of 2.9 ± 0.2 ms, matching the simulation value.

One important feature of PFCS is that the concentration of the species of interest does not affect the correlation obtained, except for the total experimental time it takes to obtain the correlation. The purity obtained (93%) for the correlation amplitude of Species 1 is lower than 100% since the contaminating, fluctuating background is always present. This upper limit on purity depends on the concentration and brightness of Species 2 and on the brightness of Species 1, but not on the concentration of Species 1. As long as bursts are able to be identified, purified correlations may be obtained. For example, if we reduce the molecular occupancy of Species 1 from 0.02 to 0.005, the amplitude of the autocorrelation of the FRET channel decreases from $A_1 = 24.5$ kHz^2 to $A_1 = 6.3$ kHz^2. Under these conditions, only 20% of the correlation amplitude comes from Species 1, and the measured diffusion time is 1.1 ± 0.1 ms, close to the diffusion time of Species 2. Using PFCS, the amplitude increases to $A_1 = 172$ kHz^2. Hence, Species 1 comprises 92% of the PFCS correlation amplitude (nearly identical to the 93% obtained above), and the diffusion time extracted is 2.8 ± 0.2 ms, close to the simulation value for Species 1.

We have demonstrated that PFCS can purify correlations for species present at single molecule concentrations with a distinguishing parameter. PFCS can also purify correlations when a low-intensity fluctuating background (caused by leakage of other fluorescence signals) is present. Unfortunately, there is currently no elegant, general theory for analyzing the effects of burst analysis on calculated correlations. This makes a quantitative theory of PFCS difficult to obtain. In place of such a general theory, we

recreate experimental situations in simulations, and test for the accuracy of the PFCS methodology. For new experimental situations that differ significantly from the above simulations, it will be necessary to perform new simulations that match those conditions. One example is applying PFCS to species that are not as well separated by the *E* histogram, such as the folded and unfolded states of proteins (20).

Biases in fitted parameters using purified FCS

We now show that, for reasonable burst search thresholds, there are no large biases in the extracted fitting parameters. A previous work (21) describes how the detected diffusion time for a single burst depends on the threshold. High thresholds tend to increase the detected diffusion time, since bursts with larger numbers of photons tend to be those events that stayed in the detection volume longer. This implies that, for PFCS, there is a balance between selectivity from a higher threshold and lower bias obtained with a lower threshold. We investigate here the effects of the burst search threshold on PFCS. We also investigate the use of our expanded burst selection regions for the Photon-arrival Interval Distribution (PAID) function (16), which adds an additional dimension of photon counts to the correlation function.

In Figure 3, we illustrate the biasing effects of burst selection on fitted parameters. In order to quantitatively analyze bias, the simulation in this example contains only a single species. Ten simulations of 60 s each were performed with molecular occupancy c=0.1, diffusion time τ_D=3 ms, brightness q=35 kHz, and background k_{bkgd}=1 kHz. We plot the fitted parameters as a function of burst search threshold, ranging from 5 kHz to 45 kHz over 10 ms bins (Figures 3a-3d). For fitted diffusion time τ_D and brightness q, an upward bias is seen as the threshold is raised, both in FCS and PAID fits (Figure 3b). However, this bias is small (within 5%) even for a significant threshold (up to 15 kHz). Hence, purified FCS and PAID do not introduce unreasonable bias in the fitted parameters as long as the burst search threshold is below the average burst intensity.

In Figure 3c, we plot the fitted occupancy c from PFCS and purified PAID, and fitted background level k_{bkgd} from purified PAID. FCS values for c are higher since FCS cannot distinguish between increases in k_{bkgd} and increases in c. The fitted occupancy values are less consistent than the values for τ_D and q. This is not surprising, since the mean and variance of the signal intensities are affected by the correlation region selection process, and FCS detects the molecular occupancy by comparing the variance of the signal intensity with the signal mean. The fitted background from PAID drops off nearly linearly, vanishing at high thresholds. Since we are excluding regions that contain only background, this is not surprising. The fitted correction factor a decreases as the threshold is raised (Figure 3d). The χ^2 values for the fits are near 1 for all of the FCS fits. However, the χ^2 for PAID increases to high values for higher thresholds. The burst selection changes the shape of the PAID function (see Figures 3e and 3f). The largest change is a decrease in the correlation amplitude to the lower right of the main peak, accounting for the lower fitted value for k_{bkgd}. The main peak is largely unchanged, accounting for the slow change in q with threshold. The changes are due to the exclusion of regions with only background. Although Figure 3b shows that purified PAID may be

used to extract accurate values of τ_D and brightness q for a single species, analysis of multiple subspecies with different q cannot be performed unless the PAID function model is changed to account for the burst selection.

Cross-correlations are often used in FCS to determine binding of two labeled, interacting molecules (7). In SMFS, ratios of fluorescence intensities from single bursts have also been used to determine the extent of binding (22). It is possible to use PFCS to select a species using ratios from SMFS, and to calculate cross-correlations of that species. We find that the selection of bursts with a specific ratio does not introduce spurious cross-correlations for time scales below the burst search time scale, allowing PFCS to distinguish bound molecules from random coincidence.

Figure 4 shows the effects of burst selection on cross-correlation experiments. Two sets of ten simulations of 60 s each with three species were performed. There are two detection channels A and B, with background levels $k_{A,\mathrm{bkgd}} = k_{B,\mathrm{bkgd}} = 1$ kHz. In both sets of simulations, Species 1 is present with molecular occupancy $c_1 = 0.05$, diffusion time $\tau_{D,1}$=3 ms, brightness $q_{A,1}$=35 kHz in Channel 1 and $q_{B,1}$=0 kHz in Channel 2. For Species 2, $c_2 = 0.05$, $q_{A,2}$=0 kHz, $q_{B,2}$=35 kHz, and $\tau_{D,2}$=3 ms. Species 3 simulates binding of Species 1 with Species 2, with $q_{A,3}$=35 kHz and $q_{B,3}$=35 kHz, and $\tau_{D,3}$=3 ms. In the first set of simulations, $c_3 = 0$; in the second set, $c_3 = 0.005$. The burst search routine searched for consecutive 10 ms time bins where the sum of counts for both channels is above 5 kHz. In the first set of simulations, there are two species that emit only in one channel each, with no crosstalk. The ratio of the intensity in one channel over the sum of both channels, $r = I_A / (I_A + I_B)$, is a bimodal distribution (gray line, figure 4b). The events with $0.3<r<0.7$ are caused by random coincidence. In the second set of experiments, a third, minor species depicting bound molecules of Species 1 and 2 was added that emits in both channels equally (black line, figure 4b). A small peak in r near 0.5 is observed.

A cross-correlation of the whole experiment produces a flat line for the first set of simulations (i.e., no cross-correlation, the dotted gray line in Figure 4b), and a positive correlation for the second set of simulations (dotted black line in Figure 4b). We first select only those bursts with $0.3<r<0.7$, but do not further exclude any regions that contain other bursts outside this range in r. The first set of simulations produces a flat line (solid gray line), and the second set of simulations produces a positive correlation (solid black line). The gray line is above 1.0 because of the modified normalization as discussed earlier. There is a drop in the cross-correlation at long time scales (> 10 ms) that is introduced by the burst selection. Even if the coincidence of bursts in both channels is only due to random coincidence, the cross-correlation can detect this as revealed by the drop at long time scales (solid gray line). Although this must be accounted for in any experiments, it is easily distinguished from an actual cross-correlation signal; a real cross-correlation caused by molecular binding also contains the correlation with the diffusion time scale (solid black line). If we now selected the bursts with $0.3<r<0.7$, and further exclude regions with other bursts with $r>0.7$ or $r<0.3$, we obtain the light gray line. This line is further above 1.0 than the gray line, and also shows

a larger drop in the cross-correlation beyond 10 ms. However, in all cases, the cross-correlations of the first set of simulations are clearly distinguished from those of the second set of simulations. No spurious cross-correlations are introduced by purified analysis of cross-correlations at or below the diffusion time. However, the increase in the constant level as well as a drop in correlation at long times (beyond the burst width time) must be accounted for.

Although it is necessary to consider the biases in any use of this methodology, the results in this section indicate that these issues will not change the extracted results more than 10% as long as the burst search threshold is below the average burst intensity.

Single-molecule FCS

Is it possible to get meaningful fits of correlation functions for regions containing only a single burst? It is not possible to get arbitrarily precise estimates of diffusion times for one single-molecule transit across the optical detection volume. Even arbitrarily strong signals will not help: FCS is a statistical method, and requires averaging over many such single-molecule transits to obtain a precise estimate of the diffusion time (21). However, as shown in figure 5, it is possible to obtain meaningful estimates of the diffusion by fitting correlation functions for single-molecule bursts when we expand the correlation region as described in figure 2.

The means of the distributions match the diffusion times of the simulation parameters. Fitting the distributions with a log-normal distribution, the standard deviation of distributions is 0.52±0.05 in units of $\ln(\tau_D)$. The full-width half maximum values for the distributions are about 0.5 in units of $\log_{10}(\tau_D)$. For species 1, the log-normal fit results in a central value of 3.2±0.2 ms. For species 2 in the donor channel, the log-normal fit results in a central value of 5.4±0.3 ms. This is the same as for the FRET channel (5-fold dimmer), where the log-normal fit results in a central value of 5.7±0.3 ms. Hence, the width of the distribution is not limited by signal-to-noise, but by having only one transit through the detection volume.

Such single-molecule FCS analysis is useful for detecting subpopulations with large differences in diffusion time. Standard FCS analysis can do similar analysis using multi-component fits, but it is often difficult to determine if the multiple time scales seen are really due to multiple species or are due to photophysical dynamics of a single species. The single-molecule FCS analysis introduced here allows these two cases to be distinguished.

The correlation function does not use the full information available in the photon stream. One way to improve on single molecule FCS is to take advantage of more of this information. For example, analysis with a recursive Bayesian estimator would likely produce improved measurements of τ_D for a single molecule event (23).

Materials and Methods

Simulations

The simulations are performed as described previously (16). A Gaussian detection volume was used in all cases, with transverse width of 0.35 μm, and longitudinal width of 1.75 μm. The 3D simulation box is of size 3.5 X 3.5 X 17.5 μm^3, with periodic boundary conditions (a molecule that leaves one side reappears at the opposite side with the same lateral position).

Single-molecule confocal fluorescence microscopy

Solution-based single molecule measurements are performed as in (6). The alternating-laser excitation experiments were performed using the 488 nm line of an Argon ion laser (Innova 90C, Coherent Inc., Santa Clara, California) and the 633 nm line of a Helium-Neon laser (1163P, Uniphase, Milpitas, California). The lasers are turned on and off using TTL timing pulses and an acousto-optic modulator (AOTF 48062-2.5-.55, NEOS technologies, West Melbourne, Florida) rather than electro-optic modulators as used previously. The alternation period is set at 25 μs.

The excitation light is reflected using a custom dichroic mirror (488-633 DBDR, Omega Optical, Brattleboro, Vermont). A 1.4 NA oil-immersion objective (60X 1.4 NA oil immersion Plan Apochromat, Nikon, Tokyo, Japan) mounted on a Nikon TE300 inverted confocal microscope is used for the excitation; a 100 μm pinhole is used on the emission detection path. The emission is split using a second dichroic mirror (580 DRLP, Omega Optical). The donor channel (for Alexa 488) is filtered using a bandpass filter (535DF45, Omega Optical), and the acceptor channel (for Alexa 647) is filtered using a longpass filter (665AGLP, Omega Optical). The photodetectors, timing electronics, and software are as described previously (6). A neutral density (ND) filter (OD 1.2) is placed in front of the detector for the donor channel to reduce the signal intensity from the donor-labeled β clamp. We time every photon, and without the ND filter our data acquisition was producing enormous files with uninteresting data produced by the donor channel. We still needed to monitor the donor channel to watch for β-clamp aggregates (see Figure 6), but we did so with a much reduced count rate.

Median-based background subtraction and burst searches

In processing the single-molecule signals and performing burst searches, we use a median-based background subtraction. A time trace with 10 ms time resolution is formed from the photon streams obtained from the single molecule microscope. At each time point, the background is determined by calculating the median of the previous 100 time bins. The median is used to avoid weighting the bursts in the signal too much in the calculation of the background. This background estimate is subtracted from each time point.

Obtaining error estimates using the bootstrap

We use a bootstrapping methodology to obtain error estimates for our fits of the purified correlation functions (16, 24). In calculating the correlation, we average the correlation

for all N_{burst} regions of interest surrounding selected bursts according to Eq. (5). For each correlation, we calculate 50 bootstrap instances of the correlations using the following procedure. We randomly select *with replacement* N_{burst} regions of interest from all N_{burst} regions of interest. Because we randomly select *with replacement*, a particular region of interest may be selected multiple times, or not at all. Using Eq. (5), we average the N_{burst} randomly selected regions of interest and obtain a bootstrap instance. Each bootstrap instance will have some regions missing, and some present twice or more. This allows the resulting bootstrap correlations to mimic additional experiments with similar noise characteristics. Using all 50 bootstrap instances, we calculate the variance for correlation time bin, and use this in weighting the fits for the correlation functions. Also, we fit each of the bootstrap instances to provide error bars for the fitted values.

DNA substrates

Analytical HPLC was performed on a HP1100 series instrument with 220 and 280 nm detection using a Vydac C18 column (5 micron, 4.6 x 150 mm) at a flow rate of 1 mL/min. All runs used linear gradients of 0.1% aqueous trifluoroacetic acid (TFA) (solvent A) *vs.* 0.1% TFA, 90% acetonitrile in H_2O (solvent B). Ultraviolet-visible (UV-vis) spectroscopy was carried out on an Agilent 8453 diode array spectrophotometer. Electrospray mass spectrometry (ES-MS) analysis was routinely applied to all compounds and components of reaction mixtures. ES-MS was performed on a Sciex API-150EX single quadrupole electrospray mass spectrometer. Calculated masses were obtained by using ChemDraw 7.0.1 or ProMac v1.5.3. Fluorescently labeled oligonucleotides were purchased from Invitrogen (Carlsbad, CA) or IDT (Skokie, IL) and purified by reverse phase HPLC. Fluorescent dyes were purchased from Invitrogen (Carlsbad, CA). Bio-Gel A-15m agarose was purchased from Bio-Rad. All other chemicals were obtained from Aldrich (Milwaukee, WI) unless otherwise indicated.

M13mp18 phage was prepared by two consecutive bandings in cesium chloride as described (25). ssDNA M13 plasmids with single hybridized DNA oligomers were prepared by annealing the synthetic DNA oligomers to purified single-stranded M13mp18 DNA as described in (26). Briefly, 9 pmol of DNA oligomer(s) were added to 45 pmol of ssDNA template in buffer A (10 mM Tris-HCl, 300 mM NaCl, pH 8) and the final volume was adjusted to 500 ml. The reaction mixture was heated to 100 ^{o}C for 5 min and slowly cooled to room temperature over 1 hr. The reaction mixture was applied to 5 ml column on Bio-Gel A-15m equilibrated in buffer B (20 mM Tris-HCl, 150 mM NaCl, pH 7.4). Fractions of 100 μl was collected and analyzed for UV absorption using spectrophotometer (Agilent, Palo Alto, California). The molar concentration of M13 ssDNA with annealed DNA oligomer was calculated using known molar absorption coefficient.

DNA hybridization experiments

Single-molecule samples are prepared by diluting DNA oligomers hybridized to ssDNA plasmids to ~100 pM concentration in a 20 mM 7.5 pH Tris buffer with 0.1 mM EDTA, 4% glycerol, 40 μg/ml BSA, 8 mM $MgCl_2$, and 50 mM NaCl. A well is formed by using

silicone well (Grace Biolabs, Bend, Oregon) on a coverslip. 10 µl of sample is placed in the well, and a second coverslip is placed on top. The solutions are monitored using the single-molecule fluorescence microscope for 5 minutes with 70 µW excitation from the 633 nm laser.

In the experiments of figure 7a, three sample solutions were prepared: one with ~100 pM of labeled, DNA oligomer hybridized to ssDNA plasmid (excess plasmid); a second with ~100 pM of labeled DNA oligomer without plasmid; a third mixture sample prerpared as a 1:1 mixture of the previous two samples. The samples were observed before and after heating at 37 ºC for 10 min. In the experiments of figure 7c, the sample with ~100 pM DNA oligomer hybridized to ssDNA plasmid (excess DNA oligomer) were observed before and after heating at 37 ºC for 10 min.

Cloning and bacterial expression of β clamp

The gene fragment encoding DNA β clamp was amplified by polymerase chain reaction (PCR) using *E. coli* K12 genomic DNA as template. The 5'-DNA primer (5'- GGT GGT CAT ATG AAA TTT ACC GTA GAA CGT GAG CAT TTA TTA AAA -3') and the 3'-primer (5'- GGT GGT TGC TCT TCC GCA GCC CAG TCT CAT TGG CAT GAC AAC ATA -3') introduced *Nde* I and *Sap* I restriction sites, respectively. The PCR amplified DNA was purified, digested simultaneously with *Nde* I and *Sap* I and then ligated into a *Nde* I, *Sap* I -treated pTXB1 plasmid (New England Biolabs, Ipswich, Massachusetts). The resulting pEY10 plasmid was shown to be free of mutations in the β clamp-coding region by DNA sequencing.

Bacterial expression was carried out as follows. *E. coli* BL21 (DE3) pLysS cells (Novagen) were transformed with pEY10. Cells were grown at 37°C to mid-log phase (OD_{600} ≈0.6) in Luria-Bertani (LB) medium and induced with 0.2 mM IPTG (isopropyl β-D-thiogalactopyranoside) at 30°C for 6 h. Cells were collected by centrifugation at 5,000 rpm in a GS3 rotor for 10 min. The cell pellet from 1 L of bacterial culture was resuspended in 20 mL of lysis buffer (0.1 mM EDTA, 1 mM PMSF, 25 mM sodium phosphate, 150 mM NaCl buffer at pH 7.4 containing 10% glycerol) and lysed by sonication. The lysate was clarified by centrifugation at 14,000 rpm in a SS-34 rotor for 30 min. The clarified supernatant (*ca*. 20 mL) containing the β clamp-Gyrase intein fusion protein was incubated with 5 mL of chitin beads (New England Biolabs) at 4°C for 1 h with gently shaking. The chitin beads were washed with 50 mL column buffer (0.1 mM EDTA, 50 mM sodium phosphate, 250 mM NaCl buffer at pH 7.2) containing 0.1% Triton X-100 then equilibrated with column buffer. The fusion protein adsorbed on the beads was subsequently cleaved with 100 mM NH_2OH in PBS at pH 7.0 (≈6 mL) for overnight at 18°C to yield free β clamp. The protein was further purified by FPLC on a MonoQ 5/50 GL column (Pharmacia) using a flow rate of 0.5 mL/min and a linear gradient from 0 to 500 mM NaCl in 50 mM Tris•HCl buffer at pH 8. The purified β clamp was characterized as the desired product by ES-MS [Expected mass (average isotopic composition) = 40642 Da; measured MW: 40659 ± 15 Da). The isolated yield for purified β clamp was around 20 mg/L.

Fluorescence labeling reaction: 15 µl of Alexa488-maleimide in DMF (1 mg/100 µl) was added to 500 µl of 50 µM β clamp in PBS (50 mM phosphate, 150 mM NaCl, 2 mM

TCEP, pH 7). The reaction was allowed to proceed for 2 hr in the dark at room temperature. Excess glutathione was added to terminate the reaction and the reaction mixture was applied to Sephadex G-25 gel filtration column and then eluted with buffer B in order to separate β clamp from the small molecular weight reactant. The reaction resulted in approximately 10% of fluorescently labeled β clamp and, under this condition, no multiple labeling was observed.

Loading of β clamp on DNA

The loading of the β clamp is performed as in (27), but with a lower concentration of DNA and β clamp. Briefly, a 100 μl reaction mixture was formed in a 20 mM 7.5 pH Tris buffer with 0.1 mM EDTA, 4% glycerol, 40 μg/ml BSA, 8 mM $MgCl_2$, and 50 mM NaCl. 40 fmol of M13 plasmid with annealed DNA olgimoer (described above) is added with 220 pmol of single-stranded binding protein (SSB). 0.4 pmol of γ clamp loading complex and 1 pmol of β-clamp (labeled monomer) are then added. Finally ATP is added to a final concentration of 1 mM. 50 μl of this reaction mixture is placed in well formed in a cell incubation chamber (WillCo-dish GWSt-3522, WillCo Wells BV, Amsterdam, The Netherlands) with silicone gasket (Grace biolabs). The solution is covered with a coverslip and is heated from room temperature to 35 ± 2 ºC over a period of 2 minutes using a microscope-based heater (Warner Instruments, Hamden, Connecticut). ALEX-based single-molecule spectroscopy is then performed for 20 minutes at 35 ± 2 ºC.

Results and Discussion

Purified FCS and the analysis of β clamp-DNA complexes

We now apply purified FCS to β clamp-DNA interaction experiments mentioned in the introduction. As seen in the time traces in Figure 6, we use a relatively high concentration (10 nM) of donor-labeled β clamp protein (from an even higher, 100 nM concentration of protein, 90% of which is unlabeled), and a low concentration (500 pM) of acceptor-labeled DNA oligomers hybridized to ssDNA plasmids. The β clamp protein forms a dimer, so that we have 10 nM of donor labeled β clamp dimer, implying that 20% of the dimers are labeled with only one donor. There is a neutral density "ND" filter on the donor channel to reduce the signal intensity on the donor channel. Thus, there are four potential fluorescent species: labeled DNA oligomers free in solution, labeled DNA oligomers annealed/hybridized to ssDNA plasmids, labeled β clamp free in solution (in dimeric form and occasional aggregates), and labeled β clamp on DNA. Individual events are easily distinguished in time traces of the emission in the FRET (black) and acceptor (red) channels, but individual events corresponding to single β clamp molecules are not identifiable since their concentration is too high. Bursts from complexes undergoing FRET (as in Figure 6a) are easily distinguished from β clamp aggregate events leaking into the FRET channel (as in Figure 6b) by looking for coincident bursts in the donor channel (implies aggregates) or in the acceptor channel (implies complexes with FRET). Then, based on ratiometric expressions calculated using these signals, we select correlation regions containing only bursts from complexes undergoing FRET. For each selected burst, the correlation regions are expanded to include 100 ms before and

after the burst. Correlations are calculated for each correlation region, and summed over all selected bursts.

The autocorrelation of the FRET channel (black and red lines in Figure 6c) found using PFCS is significantly different from the autocorrelation of the FRET channel calculated for the entire experiment (blue vs. green lines in Figure 6c). The purified FCS FRET autocorrelation is well fit Equation (2) with a diffusion time of 4.0±0.6 ms. In contrast, the FRET autocorrelation for the whole experiment is poorly fit by Equation (2) with a diffusion time of 2.0±0.2 ms. The shorter diffusion time is due to contributions from leakage of the donor signal into the FRET channel (the β clamp diffuses more quickly than the plasmid). Out of the 159 bursts in the FRET channel detected in this experiment, 21 were excluded because there was a coincident large burst in the D channel, indicating that the burst was likely a β clamp aggregate. The measured diffusion time for the excluded bursts was 3±1 ms. They were typically dimmer than the selected bursts, so these aggregates do not account for the difference in the above measured diffusion times. It appears that the primary benefit of PFCS was to exclude the dimmer, but more consistent leakage signal from free, non-aggregated β clamp, which accounts for a consistent, though fluctuating source of background photons collected in the FRET channel throughout the experiment.

Tables 1 and 2 show the effects of PFCS on the various auto- and cross-correlations calculated for this data set. Table 1 shows values for molecular occupancy, diffusion time, and brightness in three channels as extracted using PAID (16). Using PAID, we were able to extract diffusion times for each species, but the full autocorrelation was not able to be viewed independently from the other species. This ability, provided by PFCS, will be necessary for our application monitoring the movement of the DNA sliding clamp on DNA. Table 2 shows the contribution to the correlation amplitudes, or the numerator in Equation (1), of each species in Table 1. First, the contributions are shown for the entire experiment. Second, the contributions are shown after PFCS is used to select for species 4, the DNA sliding clamp-DNA complexes undergoing FRET. The bolded values are for species 4. The contribution of these complexes to the autocorrelation of the FRET channel, which is of primary interest to us, is seen to increase from 60% to 91%.

Could the difference in diffusion times measured be an artifact of the burst selection? In addition to the simulation results above, several lines of reasoning indicate that it is not. First, the diffusion of the β clamp - DNA complexes is expected to be characterized by a single diffusion time, and the PFCS autocorrelation of the FRET channel fits better to a single-component FCS model of Equation (2) than the autocorrelation of the FRET channel for the whole experiment. Second, the PFCS cross-correlation is much more consistent with the total cross-correlations between the FRET channel and acceptor channel from the DNA oligomers hybridized to ssDNA plasmids (Figure 6d). The PFCS cross-correlation fits to Equation (2) with a diffusion time of 6.4±1.1 ms, and the cross-correlation for the whole file fits well to Equation (2) with a diffusion time of 7.4±0.4 ms, equivalent to within error. In this cross-correlation case (as mentioned in the introduction), there are only two contributing signals: complexes undergoing FRET and direct excitation of lone DNA oligomers hybridized to ssDNA plasmids by the donor

excitation laser. Both have similar diffusion time scales, and we expect cross-correlations for the whole experiment to match cross-correlations obtained with PFCS.

Third, the time scale for the PFCS autocorrelation of the FRET channel makes more sense compared to the diffusion time measured for the plasmid using the acceptor excitation laser (9.6±0.4 ms). The detection volumes for the donor and acceptor excitation lasers are not the same, so we do not expect identical diffusion time values to be found in the two results. However, the diffusion times for the cross-correlation between FRET and acceptor channels should be halfway in between the diffusion times for the autocorrelations of the FRET and acceptor channels (7). If we use the value of 9.6±0.4 ms for the acceptor autocorrelation, and 7.4±0.4 ms for the cross-correlation, we expect an autocorrelation diffusion time of 5.2±0.6 ms. Within error, this matches the value of 4.0±0.6 ms from the purified correlation analysis much better than the 2.0±0.2 ms value extracted from the entire experiment.

As shown in this example, purified FCS with the correlation region expansion allows us to monitor the temporal dynamics of individual species even in the presence of other species. Using this methodology, we are studying the motion of the β clamp protein on DNA (manuscript in preparation).

Single-molecule FCS and DNA hybridization

In our initial β clamp experiments, we incubated the reaction mixture for 10 minutes at 37 ºC before spectroscopy (in later measurements the sample was heated on the microscope). In these first experiments, we noticed that the diffusion time measured in the acceptor channel decreased significantly after incubation. This was an apparent paradox since the signal in the acceptor channel should be exclusively from the labeled DNA oligomers annealed to ssDNA plasmids, which should not be affected by gentle heating or by loading of the β clamp. A clue was that we found the change in diffusion time after heating occurred even without the β clamp or clamp loading complex. FCS measurements (not shown) suggested two components, one with a long diffusion time (3.5 ms) and one with a short diffusion time (0.7 ms). The strength of the component with the shorter diffusion time increased after heating. By standard FCS, however, there is an ambiguity as to how much of the deviation from a one-component fit is due to a second diffusing species and how much is due to internal dynamics of the large DNA (28, 29). Single-molecule FCS provides a way to show that there are indeed two diffusing components with different diffusion times.

Using single molecule FCS, we found that the change in diffusion time was due to unbinding of labeled 30mer DNA oligomers weakly bound to the ssDNA plasmid. We annealed the short DNA oligomers to the ssDNA plasmid using a 10:1 excess of DNA oligomers in order to be sure that each ssDNA plasmid was hybridized by a DNA oligomer. Depending on the sequence specificity of the short DNA oligomers, multiple DNA oligomers can be attached to a DNA plasmid at 40ºC, as seen previously in FCS experiments under similar conditions (30). We hypothesize, therefore, that additional DNA oligomers are likely attached to the ssDNA plasmid at the lower temperature we used for purification, and detach from the ssDNA plasmid upon heating of the DNA oligomer-plasmid complexes to 37ºC.

In Figure 7a, we show that single-molecule FCS distinguishes between free 30mer DNA oligomers and 30mer DNA oligomers attached to ssDNA plasmids. The 30mer is labeled with Alexa647 dye at the 5′ end. The green line in Figure 7a is the histogram for a solution with free 30mer DNA oligomers. The red line is the histogram for DNA oligomers attached to plasmid, prepared using a 5:1 excess of plasmid to prevent attachment of weakly bound DNA oligomers. The black line is the histogram for a solution formed as a 1:1 mixture of the pure samples. The histogram for the mixture can be accurately predicted simply by averaging the results for the two pure samples (blue line). All of these histograms remain the same after heating to 37ºC (not shown).

As can be seen by comparing results from figures 7a and 7b, single-molecule FCS produces a better separation of species than can be obtained by using histograms of single-molecule burst widths. In comparing the histograms, one must keep in mind that the faster diffusing species produces more bursts than the slower diffusing species for the same concentrations. In figure 7a, even though more burst are detected from the faster diffusing species, the slower diffusing DNA oligomers attached to ssDNA plasmids are at a higher concentration. See figure 1S in the supplementary information to see histograms corrected for this effect.

Since we measured the histograms produced by the free DNA oligomers alone and the DNA oligomers bound to the ssDNA plasmids alone, we can calculate the probability that the burst identification is correct in the 1:1 mixture sample. If, for the extracted diffusion time of a given burst, there were more bursts in the free DNA oligomer histogram, then most likely the burst was from that species. If there were more bursts in the histogram for DNA oligomers bound to the ssDNA plasmid, then most likely the burst was from that species. For a burst with a specific diffusion time, the probability that the species identification is correct is the ratio of the maximal number of bursts in one histogram with that diffusion time divided by the sum of the number of bursts for in the histograms for both species with that diffusion time. This probability is plotted in figure 7a as the cyan curve. A corresponding plot is shown in figure 7b using burst widths. As can be seen, the probability of correct identification is significantly larger using single molecule FCS than by using burst widths. Summing over all bursts, the probability of correct identification using single molecule FCS is calculated to be 92%. For burst widths, the probability is 72%.

Now, suppose we did not use any of this information, and only used the total number of bursts in the individual species histograms. There were 2101 bursts in histogram for DNA oligomers bound to ssDNA plasmids, and 4900 bursts in the histogram for free DNA oligomers. Using this, we could guess, based on no other information, that any burst has a 70% chance of coming from a free DNA oligomer. Hence, we see that the information gain in the case of burst widths is minimal, only 2%. For longer burst widths, there is a >95% chance that the burst comes from the slower diffusing species, but there is only minimal discrimination for shorter burst widths. However, single molecule FCS produces significant gains in information for both long and short bursts. There are single molecule diffusion times that provide >95% chance of correct species identification both for the slower and faster diffusing species.

In Figure 7c, we show the results of experiments with a 10:1 excess of labeled DNA oligomer. In this case, there is a large increase in the amount of free DNA oligomer after

the 10 minute incubation at 37 ºC. There is some decrease in the number of long-diffusion time bursts, likely because these bursts are dimmer after losing weakly bound DNA oligomers. In these histograms, there are many more short diffusion-time bursts than long diffusion time bursts. Here, there is about a factor of 5 difference in the diffusion times of the labeled DNA oligomer and DNA oligomers hybridized to ssDNA plasmids, leading to a factor of 5 more bursts from the labeled DNA oligomer even with the same concentration.

Conclusion

We have shown that purified FCS allows correlation analysis on individual subpopulations selected using single molecule measurements. We can use standard FCS models by expanding the region of interest around the detected bursts. This methodology will be useful in purifying correlations for species of interest. This will help improve our ability to apply FCS and single-molecule analysis to questions involving fast fluctuations in rare species.

Additionally, we have demonstrated single molecule FCS analysis that may be used to distinguish between bursts from species with at least a 5-fold difference in diffusion times. Here we showed that weakly bound DNA oligomers can fall off ssDNA plasmids even with gentle heating at 37 ºC. This methodology can be further used for measuring binding kinetics of large proteins/DNA with smaller proteins, DNA, or small molecules. These results indicate that, although the amount of information from single molecules bursts is finite (31), we have not yet taken full advantage of the information that is there.

Acknowledgments

This work was performed under the auspices of the U.S. Department of Energy by the University of California, Lawrence Livermore National Laboratory under Contract No. W-7405-Eng-48. This work was supported by the laboratory directed research and development (LDRD) program at LLNL. We thank the laboratory of Professor Mike O'Donnell of Rockefeller University for supplying us with β clamp, ssDNA plasmids, SSB, and clamp loader γ. We thank Professor Thomas Huser of UC Davis Medical Center for critically reading the manuscript.

References

1. Magde, D., E. Elson, and W. W. Webb. 1972. Thermodynamic fluctuations in a reacting system: measurement by fluorescence correlation spectroscopy. Phys. Rev. Lett. (USA) 29:705-708.
2. Rigler, R., and J. Widengren. 1990. Ultrasensitive detection of single molecules by fluorescence correlation spectroscopy. Bioscience 3:180-183.
3. Rigler, R., and E. Elson. 2001. Fluorescence correlation spectroscopy: theory and applications. Springer, Berlin; New York.
4. LaClair, J. J. 1997. Analysis of highly disfavored processes through pathway-specific correlated fluorescence. Proceedings Of The National Academy Of Sciences Of The United States Of America 94:1623-1628.

5. Maiti, S., U. Haupts, and W. W. Webb. 1997. Fluorescence correlation spectroscopy: diagnostics for sparse molecules. Proceedings of the National Academy of Sciences of the United States of America 94:11753-11757.
6. Kapanidis, A. N., N. K. Lee, T. A. Laurence, S. Doose, E. Margeat, and S. Weiss. 2004. Fluorescence-aided molecule sorting: analysis of structure and interactions by alternating-laser excitation of single molecules. Proc Natl Acad Sci U S A 101:8936-8941.
7. Schwille, P., F. J. Meyer-Almes, and R. Rigler. 1997. Dual-color fluorescence cross-correlation spectroscopy for multicomponent diffusional analysis in solution [see comments]. Biophysical Journal 72:1878-1886.
8. Muller, B. K., E. Zaychikov, C. Brauchle, and D. C. Lamb. 2005. Pulsed interleaved excitation. Biophysical Journal 89:3508-3522.
9. Deniz, A. A., T. A. Laurence, M. Dahan, D. S. Chemla, P. G. Schultz, and S. Weiss. 2001. Ratiometric single-molecule studies of freely diffusing biomolecules. Annu Rev Phys Chem V52:233-253.
10. Eggeling, C., J. R. Fries, L. Brand, R. Günther, and C. A. Seidel. 1998. Monitoring conformational dynamics of a single molecule by selective fluorescence spectroscopy. Proceedings of the National Academy of Sciences of the United States of America 95:1556-1561.
11. Fries, J. R., L. Brand, C. Eggeling, M. Kollner, and C. A. M. Seidel. 1998. Quantitative identification of different single molecules by selective time-resolved confocal fluorescence spectroscopy. J Phys Chem a 102:6601-6613.
12. Rothwell, P. J., S. Berger, O. Kensch, S. Felekyan, M. Antonik, B. M. Wohrl, T. Restle, R. S. Goody, and C. A. Seidel. 2003. Multiparameter single-molecule fluorescence spectroscopy reveals heterogeneity of HIV-1 reverse transcriptase:primer/template complexes. Proc Natl Acad Sci U S A 100:1655-1660.
13. Laurence, T. A., X. Kong, M. Jager, and S. Weiss. 2005. Probing structural heterogeneities and fluctuations of nucleic acids and denatured proteins. Proc Natl Acad Sci U S A 102:17348-17353.
14. Rigler, R., U. Mets, J. Widengren, and P. Kask. 1993. Fluorescence Correlation Spectroscopy With High Count Rate and Low Background - Analysis of Translational Diffusion. Eur Biophys J 22:169-175.
15. Widengren, J., U. Mets, and R. Rigler. 1995. Fluorescence Correlation Spectroscopy of Triplet States in Solution - a Theoretical and Experimental Study. J Phys Chem 99:13368-13379.
16. Laurence, T. A., A. N. Kapanidis, X. X. Kong, D. S. Chemla, and S. Weiss. 2004. Photon arrival-time interval distribution (PAID): A novel tool for analyzing molecular interactions. J Phys Chem B 108:3051-3067.
17. Deniz, A. A., M. Dahan, J. R. Grunwell, T. Ha, A. E. Faulhaber, D. S. Chemla, S. Weiss, and P. G. Schultz. 1999. Single-pair fluorescence resonance energy transfer on freely diffusing molecules: observation of Förster distance dependence and subpopulations. Proceedings of the National Academy of Sciences of the United States of America 96:3670-3675.
18. Aragon, S. R., and R. Pecora. 1976. Fluorescence correlation spectroscopy as a probe of molecular dynamics. J. Chem. Phys. (USA) 64:1791-1803.

19. Schatzel, K., M. Drewel, and S. Stimac. 1988. Photon correlation measurements at large lag times: improving statistical accuracy. J. Mod. Opt. 35:711-718.
20. Deniz, A. A., T. A. Laurence, G. S. Beligere, M. Dahan, A. B. Martin, D. S. Chemla, P. E. Dawson, P. G. Schultz, and S. Weiss. 2000. Single-molecule protein folding: diffusion fluorescence resonance energy transfer studies of the denaturation of chymotrypsin inhibitor 2. Proceedings of the National Academy of Sciences of the United States of America 97:5179-5184.
21. Enderlein, J., and M. Kollner. 1998. Comparison between time-correlated single photon counting and fluorescence correlation spectroscopy in single molecule identification. Bioimaging 6:3-13.
22. Li, H. T., D. J. Zhou, H. Browne, S. Balasubramanian, and D. Klenerman. 2004. Molecule by molecule direct and quantitative counting of antibody-protein complexes in solution. Anal Chem 76:4446-4451.
23. McHale, K., A. J. Berglund, and H. Mabuchi. 2004. Bayesian estimation for species identification in single-molecule fluorescence microscopy. Biophysical Journal 86:3409-3422.
24. Efron, B., and R. Tibshirani. 1993. An introduction to the bootstrap. Chapman & Hall, New York.
25. Turner, J., and M. O'Donnell. 1995. Cycling of Escherichia coli DNA polymerase III from one sliding clamp to another: model for lagging strand. Methods Enzymol 262:442-449.
26. Yao, N., F. P. Leu, J. Anjelkovic, J. Turner, and M. O'Donnell. 2000. DNA Structure Requirements for the Escherichia coli gamma Complex Clamp Loader and DNA Polymerase III Holoenzyme. J. Biol. Chem. 275:11440-11450.
27. Yao, N., J. Hurwitz, and M. O'Donnell. 2000. Dynamics of beta and proliferating cell nuclear antigen sliding clamps in traversing DNA secondary structure. J Biol Chem 275:1421-1432.
28. Lumma, D., S. Keller, T. Vilgis, and J. O. Radler. 2003. Dynamics of large semiflexible chains probed by fluorescence correlation spectroscopy. Phys Rev Lett 90:218301.
29. Shusterman, R., S. Alon, T. Gavrinyov, and O. Krichevsky. 2004. Monomer dynamics in double- and single-stranded DNA polymers. Phys. Rev. Lett. (USA) 92:-.
30. Kinjo, M., and R. Rigler. 1995. Ultrasensitive hybridization analysis using fluorescence correlation spectroscopy. Nucleic Acids Res 23:1795-1799.
31. Talaga, D. S. 2006. Information theoretical approach to single-molecule experimental design and interpretation. J Phys Chem A 110:9743-9757.

Tables

Table 1: Fluorescence parameters for data from Figure 6

Species		c	τ_D (ms)	q_D (kHz)	q_{FRET} (kHz)	q_A (kHz)
1	Free β clamp	2.4 ± 0.2	0.7 ± 0.1	710 ± 50	90 ± 50	0
2	β clamp Agg.	0.005 ± 0.002	2±1	3000 ± 400	600 ± 50	0
3	Free DNA	0.24 ± 0.02	8 ± 1	0	40 ± 10	1900 ± 100
4	Complexes	0.02 ± 0.01	4 ± 1	0	1200 ± 200	1900 ± 100

Table 2: Effects of PFCS on contributions to correlations (factor of 7 in concentrating sample)

Correlation	Term	FCS amplitude (kHz^2) for entire experiment				FCS amplitude (kHz^2) for complexes selected by PFCS			
		1	2	3	4	1	2	3	4
FRET Autocorr.	cq_{FRET}^2	1.9E4	1.8E3	380	2.9E4	1.9E4	0	380	**2.0E5**
Acceptor Autocorr.	cq_{A}^2	0	0	8.7E5	7.2E4	0	0	8.7E5	**5e5**
Donor Autocorr.	cq_{D}^2	1.2E6	4.5e4	0	0	1.2E6	4.5e4	0	0
FRET-Acceptor Cross.	$cq_{\mathrm{FRET}}q_{\mathrm{A}}$	0	0	1.8E4	4.6E4	0	0	1.8E4	**3E5**
FRET-Donor Cross.	$cq_{\mathrm{FRET}}q_{\mathrm{D}}$	1.5E5	9E3	0	0	1.5E5	9E3	0	0
Donor-Acceptor Cross.	$cq_{\mathrm{D}}q_{\mathrm{A}}$	0	0	0	0	0	0	0	0

Figure Captions

Figure 1: Signals contributing to a detection channel monitoring fluorescence resonance energy transfer (FRET). (a) FRET is detected by exciting the donor fluorophore and monitoring emission of the acceptor fluorophore. Absorbance (dotted lines) and emission (solid lines) are shown for Alexa 488 (Molecular Probes, gray lines) as donor (D) and Alexa 647 (Molecular Probes, black lines) as acceptor (A). The laser excitation of 488 nm is shown in light gray, and the bandpass region for the emission filter (650LP, Omega Optical) is shown in gray. (b) Leakage of D signal into the A detection channel fromthe tail of the D emission curve (solid black line) causes detectable signals that contaminate the signal in the FRET channel. (c) Direct excitation of the A molecules by the D excitation laser (488 nm) also causes signals in the FRET channel.

Figure 2: Purified fluorescence correlation spectroscopy (PFCS) of individual species is performed by selection of single-molecule bursts. In this simulation, we separate the autocorrelation of the FRET channel for Species 1 undergoing FRET from donor D to acceptor A from that of the aggregated Species 2 with multiple copies of D (with leakage into the FRET channel). (a) Time trace of simulated emission from Species 1 and 2 in donor and FRET channels. Twenty percent of the D emission (gray) leaks in to the FRET detection channel (black). (b) Histogram of uncorrected FRET efficiency ratio E (or proximity ratio) calculated for each detected burst. The peak near E=1 (dark gray shading) is from Species 1, and the peak near E=0.25 (light gray shading) is from Species 2. (c) Autocorrelations of the FRET channel calculated using selective FCS (using only photons within bursts). Black squares: autocorrelation for the whole simulation without purification. In (c) and (f), fits of data to Equation (2) are shown as solid lines of same color as data points. Dark gray triangles: selective FCS autocorrelation for bursts from Species 1. Light gray circles: selective FCS autocorrelation for bursts from Species 2. (d) In PFCS, we expand the correlation region to include photons outside the bursts, in this case 100 ms on either side of each burst. If another burst is found within this region, the region is still included in the autocorrelation as long as the burst is from the same species. (e) A region is excluded if another burst from the wrong species is present. (f) By expanding the correlation region beyond the burst, we recover the correct autocorrelations for the individual species. Black squares are the same as in (c). Dark gray triangles: PFCS autocorrelation for bursts from species 1. Light gray circles: PFCS autocorrelation for bursts from species 2.

Figure 3: Effects of burst search thresholds on fitted parameters obtained using purified FCS (PFCS) and purified PAID for simulations containing a single species. (a) Time trace of simulated fluorescence intensity with 10 ms time resolution. The burst search routine searched for consecutive time bins over a pre-determined threshold. The five thresholds used are shown as horizontal gray lines: 5, 15, 25, 35, and 45 kHz. In the following results, the points at the 0 kHz threshold are for the entire experiment. (b) Fitted τ_D using FCS (black), using PAID (red), and fitted q using PAID (green) as a function of burst search threshold. (c) Fitted c using FCS (black), using PAID (red), and

fitted k_{bkgd} using PAID as a function of burst search threshold. (d) Fitted values for the correction factor *a* using FCS (black) and PAID (red). χ^2 for FCS (blue) and PAID (green). (e) PAID histogram for entire experiment. (f) Purified PAID histogram for 15 kHz threshold.

Figure 4: Effects of PFCS burst selection on cross-correlations. In the first set of simulations, there are two species that emit only in channel A or channel B, with no crosstalk. In the second set of experiments, a third, minor species depicting bound molecules of Species 1 and 2 was added that emits in channels A and B equally. (a) Histograms of the ratio $r = I_A/(I_A + I_B)$ calculated for each detected burst (similar to *E* histogram in figure 2), where I_A and I_B are detected intensities in channels 1 and 2. The first set of simulations without species 3 is shown in gray, the second set with species 3 is shown in black. The peak near r=1 is from Species 1, and the peak near r=0 is from Species 2. The peak near r=0.5 from the second set of simulations is from species 3. (b) Cross-correlations obtained under various conditions. Dotted gray line: standard cross-correlation for first set of simulations without species 3. Gray line: PFCS on bursts with $0.3<r<0.7$ are selected, and correlation regions are expanded by 100 ms. Light gray line: PFCS on bursts with $0.3<r<0.7$ are selected, but correlation regions that also contain bursts with $r<0.3$ or $r>0.7$ are excluded. Dotted black line: standard cross-correlation for second set of simulations with species 3. Black line: PFCS on second set of simulations, bursts with $0.3<r<0.7$ are selected.

Figure 5: Extracting diffusion times found by fitting correlations of small regions around individual bursts (100 ms on either side). (a) Examples of correlations of individual burst correlation regions. Solid lines are correlations; dotted lines are fits. (b) Extracted diffusion times. The simulation is the same as used in figure 1. The x axis is the fitted diffusion time, and the y axis is the number of bursts. Three histograms are shown; fits to log-normal distributions are shown as dotted lines of same color. Black: fits for autocorrelations of channel D of bursts from Species 2 in figure 1. Gray: fits for autocorrelations of channel A of bursts from Species 2 in figure 1. For Species 2, the brightness in channel A is five times smaller than in channel D. Light gray: fits for autocorrelations of channel A of bursts from Species 1 in figure 1.

Figure 6: Purified FCS for autocorrelations of the FRET channel from complexes of D-labeled β clamps and A-labeled DNA (concentration of β clamp is larger than DNA). (a-b) Example time traces with 10 ms resolution for reaction mixtures. Green: donor emission; red: acceptor emission excited by acceptor excitation laser; black: FRET emission, or acceptor emission excited by donor excitation laser. The median count rate for the previous 100 bins is subtracted from each bin, leading to occasional negative count rates. Bursts in the red channel correspond to individual plasmids traversing the detection volume. Bursts in the green channel correspond to aggregates of beta clamp; individual beta clamps are not distinguished due to high concentrations. Bursts in the

black channel correspond to complexes exhibiting FRET (a) or leakage from aggregates in the donor channel (b). We obtain the purified autocorrelation of the FRET channel by performing correlations only over regions within 100 ms of a burst exhibiting FRET that does not have a corresponding burst in the donor channel. (c) The purified autocorrelation of the FRET channel (black line) and fit (red line) are shown. The autocorrelation of the FRET channel for the whole experiment (green line) and fit (blue line) are also shown. (d) The purified cross-correlation of the FRET channel and the acceptor channel (black line) and fit (red line) are shown. The cross-correlation of the FRET channel and the acceptor channel for the whole experiment (green line) and fit (blue line) are also shown.

Figure 7: Species with a large difference between diffusion times may be distinguished by fitting diffusion times for single-molecule burst events. Single-molecule experiments were performed on solutions containing fluorescent labeled 30-base DNA oligomers, both free and annealed to 7.2 kilobase ssDNA plasmids. (a) Annealed plasmids were prepared with a 5:1 excess of plasmid to ensure that only one DNA oligomer was annealed to each plasmid. Histograms of fitted diffusion times for single-molecule FCS with correlation regions within 100 ms of a single molecule burst are shown. Green line: ~50 pM solution of the DNA oligomers. Red line: ~100 pM solution of DNA oligomers annealed to the plasmids. Black line: 1:1 mixture of the two previous solutions. Blue line: average of histogram of single component solutions (green and red lines), predicting the expected results for the 1:1 mixture. Cyan: probability that identification of burst is correct in mixture sample (black line), calculated using histograms of individual components (green and red lines). In (b) we plot histograms of burst durations rather than fitted diffusion times. The colors refer to the same solutions (or averaged results) as in (a). Cyan: probability that identification of burst is correct in mixture sample (black line). (c) The annealed plasmids were prepared with a 10:1 excess of DNA oligomer, allowing poorly bound DNA oligomers to remain attached to the plasmid during purification. The two measurements shown (performed at room temperature) are before (black line) and after (red line) heating the solution to 37 ºC.

Figures

Figure 1:

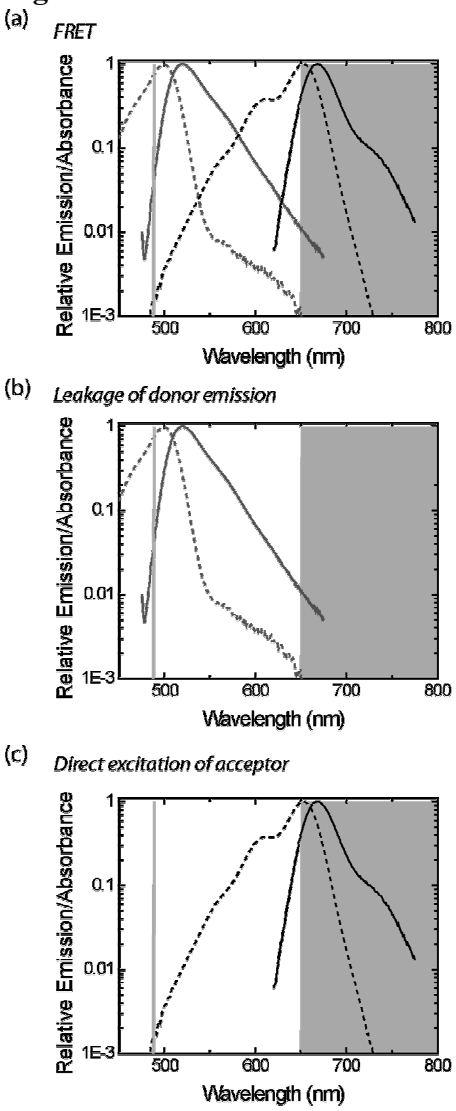

Figure 2:

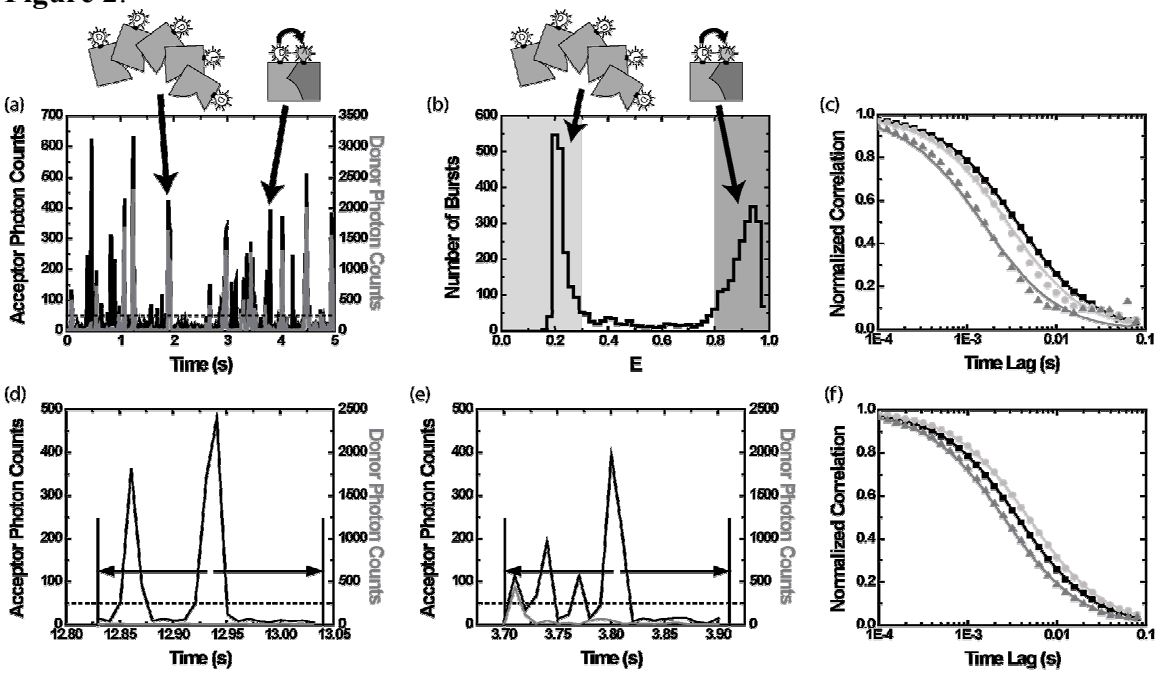
(a)
Acceptor Photon Counts
Donor Photon Counts
Time (s)
(b)
Number of Bursts
E
(c)
Normalized Correlation
Time Lag (s)
(d)
Acceptor Photon Counts
Donor Photon Counts
Time (s)
(e)
Acceptor Photon Counts
Donor Photon Counts
Time (s)
(f)
Normalized Correlation
Time Lag (s)

Figure 3:

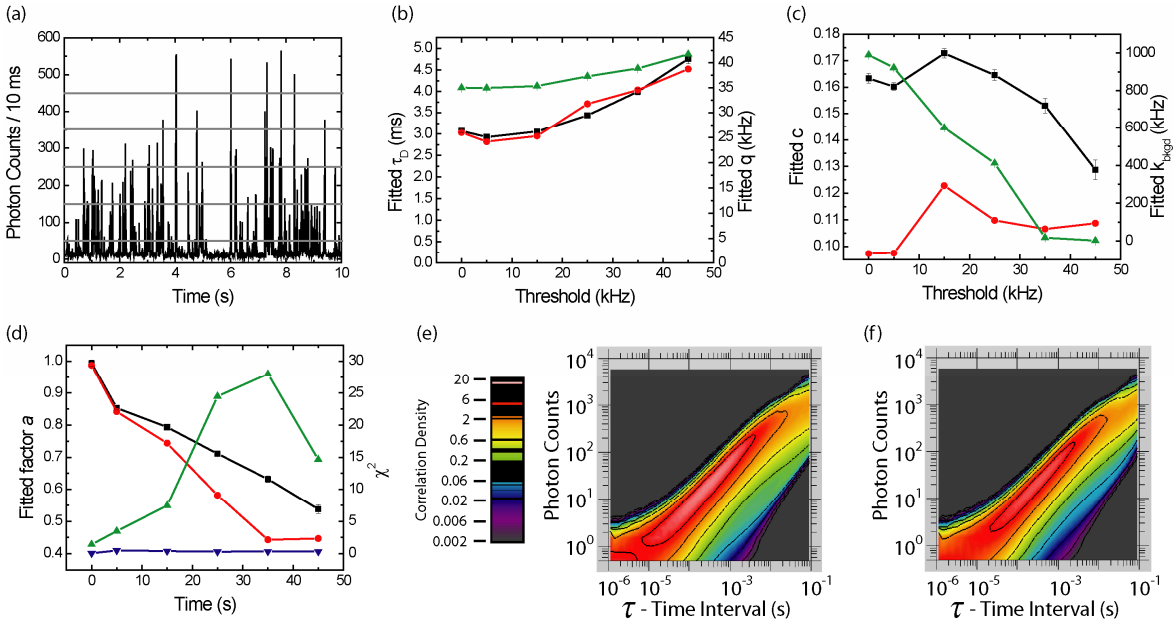
(a)
Photon Counts / 10 ms
Time (s)
(b)
Fitted τ_D (ms)
Fitted q (kHz)
Threshold (kHz)
(c)
Fitted c
Fitted k_{bgd} (kHz)
Threshold (kHz)
(d)
Fitted factor a
χ^2
Time (s)
(e)
Correlation Density
Photon Counts
τ - Time Interval (s)
(f)
Photon Counts
τ - Time Interval (s)

Figure 4:

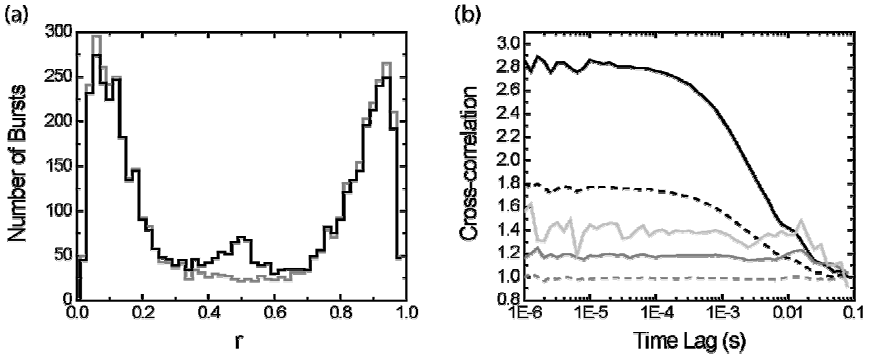

Figure 5:

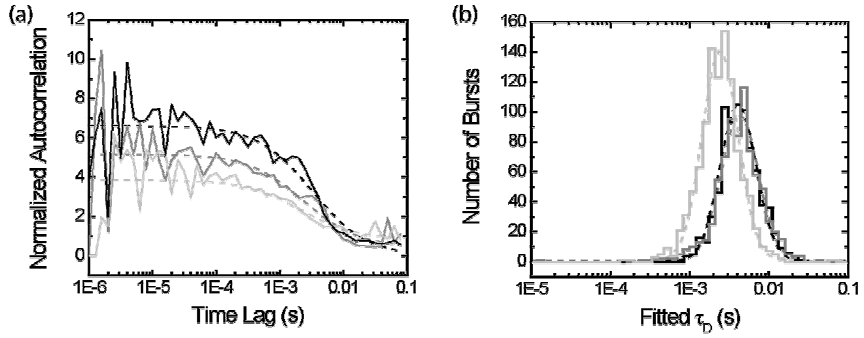
(a)
Normalized Autocorrelation
12
10
8
6
4
2
0
1E-6
1E-5
1E-4
1E-3
0.01
0.1
Time Lag (s)
(b)
Number of Bursts
160
140
120
100
80
60
40
20
0
1E-5
1E-4
1E-3
0.01
0.1
Fitted τ_D (s)

Figure 6:

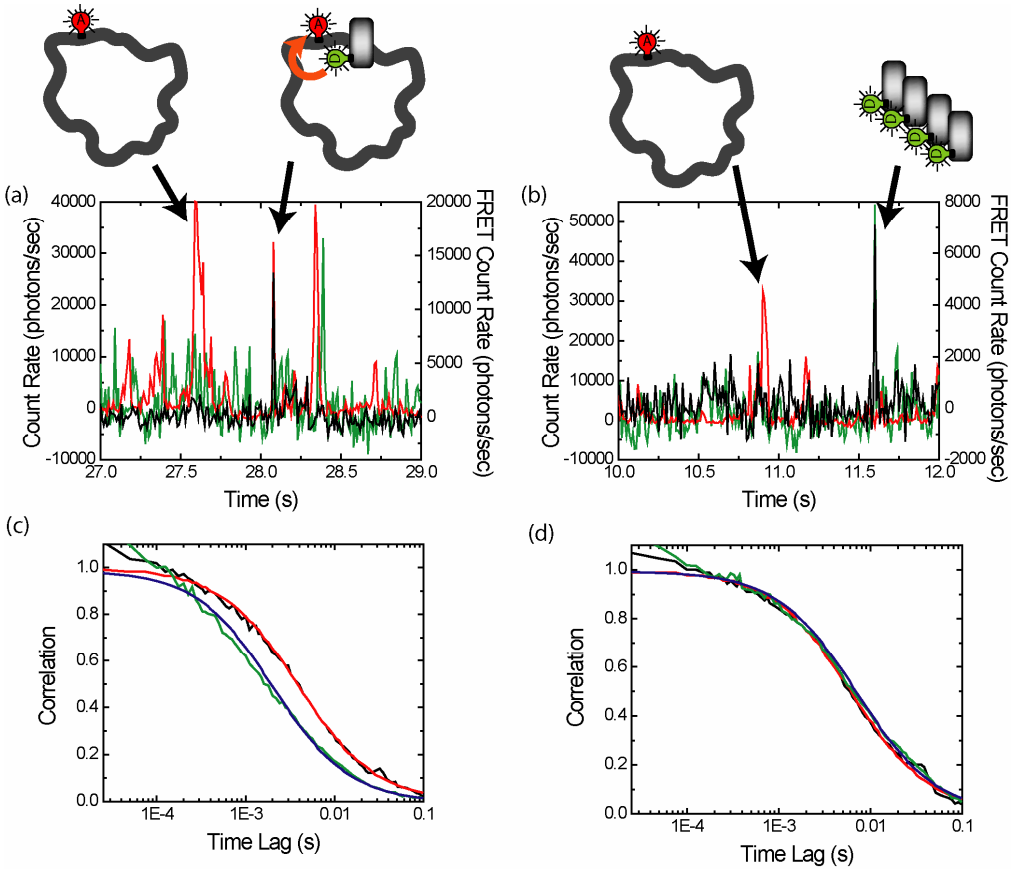
(a)
Count Rate (photons/sec)
FRET Count Rate (photons/sec)
Time (s)
(b)
Count Rate (photons/sec)
FRET Count Rate (photons/sec)
Time (s)
(c)
Correlation
Time Lag (s)
(d)
Correlation
Time Lag (s)

Figure 7:

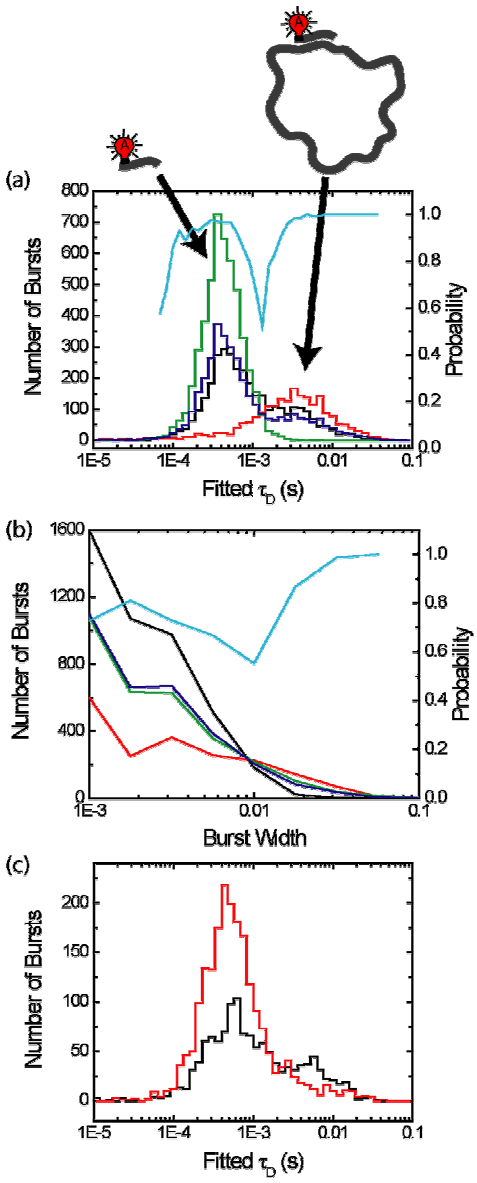
(a)
Number of Bursts
Probability
Fitted τ_D (s)
(b)
Number of Bursts
Probability
Burst Width
(c)
Number of Bursts
Fitted τ_D (s)